





## Research Article

# Influence of Decoupled Charge Structure and Filler on the Blasting Effect

Yiping Zhang , Yi Luo , Sipeng Wan , Yingxiang Tian , Huanchao Ding ,  
Xiaoxiao Zhang , Chengcheng Fang , and Yuyao Zhang 

*College of Mining, Guizhou University, Guiyang, Guizhou 550025, China*

Correspondence should be addressed to Yi Luo; [gzu\\_yiluo@163.com](mailto:gzu_yiluo@163.com)

Received 30 September 2020; Revised 3 November 2020; Accepted 25 November 2020; Published 7 December 2020

Academic Editor: Guangchao Zhang

Copyright © 2020 Yiping Zhang et al. This is an open access article distributed under the Creative Commons Attribution License, which permits unrestricted use, distribution, and reproduction in any medium, provided the original work is properly cited.

This study compared models of specimens with different filler media and decoupled charge structures in terms of the blasting effect. The test system combined a high-speed camera and high-speed static strain test analyzer. A physical model of a concrete single-borehole decoupled charge structure was designed to study the geometric elements of the blasting funnel, flyrock launch velocity, peak strain values, and distribution of the gravel lumpiness. The experimental results showed that for the same decoupling coefficient, when expandable polystyrene foam (EPS) was used as the filling medium, the radius, depth, and volume of the blasting funnel of the model specimen were larger, the flyrock launch velocity was slower, the peak stress of the specimen was higher, and the distribution of gravel lumpiness was more even. The relationship between the experimental index and the decoupling coefficient follows the changing trend of first increasing and then decreasing or first decreasing and then increasing. With air and EPS as the filling media, the concrete model specimens could achieve optimal blasting effects at decoupling coefficients of 1.83 and 1.69, respectively. The results confirm the feasibility and practicability of using EPS as a filler and can provide guidance and an experimental basis for the selection of the decoupling coefficient and filling medium in blasting engineering.

## 1. Introduction

Drilling and blasting can efficiently crush rock media and are used in civil applications such as mining [1–3] and tunnel construction [4, 5]. The blasting fracture of rock can be viewed as the result of a synergistic effect of the blasting stress wave and the quasistatic pressure of the blasting gas. The blasting stress wave is the main cause of rock fracture, while the blasting gas further expands the cracks [6–8]. Efficient energy use to achieve the desired blasting effect has been extensively researched. The properties of the rock, type of explosive, initiation method, borehole layout, and charge structure all affect the blasting result; however, the charge structure is the most important factor [9].

Foster first proposed achieving directional fracture of rock using detonation energy from blasting to act on the axial groove of the drilling borehole over a hundred years ago. Limited by the theory and construction techniques, the

proposed technology of changing the charge structure [10] could not be implemented. Since their proposal in 1940, air-decoupled charge structures have been applied in many countries, achieving economic benefits in mines, water conservancy, highways, and other fields [11]. Segmented charges were later used in production, such as in the Chinese Anshan Iron and Steel Mine and the Anhui Phoenix Mine [12]. Charge structures can now be divided into coupled and decoupled charges, continuous charges, and interval charges. Decoupled charges can be further distinguished as radial, axial, and radial-and-axial structures. Water or other filling media are used in decoupled charge structures [11–13]. Different charge structures have varying influences on the energy transfer, borehole pressure, explosive stress field, and blasting effect of explosives; smooth blasting, presplit blasting, and other controlled blasting methods typically adopt decoupled charge structures [14].

A decoupled charge structure can effectively avoid excessive fragmentation of rocks around the borehole, ensure utilization of the blasting energy, and achieve the best blasting effect [15]. Thus, decoupled charge structures have been shown to perform better than coupled charge structures in engineering practice. The decoupling coefficient and filling medium [16–25] are the main factors contributing to the blasting effect. Experiments performed by Gu et al. [16] on the decoupling coefficient showed that a water-decoupled charge structure could effectively taper the instantaneous vibrational energy, resulting in a higher average crushing rate of the rock and less harmful dust. They also demonstrated the relationship between different charge structures and the corresponding rock impedance, noting that there was an optimal decoupling coefficient. Lei et al. [17] conducted comparative tests on low-permeability coal seams with three charge groups having different shapes and decoupling coefficients. When the radial decoupling coefficient was 1.5, the stress wave with a lower main frequency had the strongest stimulation effect on the coal body. Under the joint action of the blasting stress wave and detonation gas, the gas extraction rate in low-permeability coal seams can be increased by a factor of 2.0–3.4. The influence of the decoupling coefficient on explosive crack growth was studied in laboratory experiments and confirmed through numerical simulations by Wang et al. [18]. At a decoupling coefficient of 1.67, the blasting effect of a slotted charge is best. The crack growth speed and dynamic stress intensity factor decrease with vibration and reach a small peak in the middle and late stages of crack growth. A decoupled charge structure weakened the intensity of the initial blasting stress wave, and either water or mortar as a filler reduced the dissipation of the blasting energy, as demonstrated by Jiang et al. [19] for carbonate rock using ANSYS/LS-DYNA software. This result was confirmed in a comparative study of air and water by Wang et al. [20], who found that the energy dissipation was caused by excessive fragmentation of the surrounding rock by the blasting shock wave, which was limited with the use of a water filler. Yang et al. [21] investigated the impact of the filling medium and decoupling coefficient on the evolution of the blasting stress in decoupled charge blasting. With an increase in the decoupling coefficient, the blasting stress attenuation index initially increased and then decreased. In addition, numerical simulation results showed that in decoupled charge blasting, the filling medium reduced the pressure of the borehole, and the peak stress of the borehole wall was lowest when the decoupling coefficient was 2.5–3.5.

While a decoupled charge structure can improve the blasting effect, the blasting requirements vary with different environments and fillers [17, 26]. The state of research on decoupling coefficients currently consists of studies that have been previously performed, in many cases a long time ago. Owing to the anisotropy of rock materials and the experimental data collected, the analytical results vary too significantly to be predictive [27]. The authors selected a suitable model material, concrete, to derive more controlled and reliable data. To date, most studies on filling media have focused on natural materials such as air, water, sand, and soil

[28, 29]. Few studies have been conducted using polymers (e.g., expandable polystyrene foam (EPS)). Using EPS in combination with a decoupled charge structure can provide the following unique advantages [29, 30]:

- (1) EPS is solid and extremely light. Thus, no auxiliary device is needed to position the explosive in the borehole.
- (2) EPS can dissipate the stress wave to assist in decreasing the decoupling coefficient appropriately.
- (3) EPS can meet special requirements such as those for eccentric decoupled blasting and can control the vibration.

An appropriate selection of the decoupling coefficient and filling medium is important to improve the blasting effect.

## 2. Methods and Experimental Setup

*2.1. Experimental System.* A physical model of a concrete single-borehole decoupled charge blasting system was designed, and a test system combining a high-speed camera with a high-speed static strain tester was used. The following aspects were considered:

- (1) The angles of the geometric elements of the blasting funnel.
- (2) The flyrock launch velocity.
- (3) The peak strain of the specimen.
- (4) The distribution of the gravel lumpiness.
- (5) The effects of the decoupling coefficient.
- (6) The effect of the filling medium on the blasting.

The feasibility and practicability of the use of EPS as a filling medium for a decoupled charge structure are confirmed, and these results can provide reliable theoretical guidance and an experimental basis for selection of the decoupling coefficient and filling medium in blasting engineering.

The authors studied the relationship between the decoupled charge structure and the blasting effect and designed a test system combining a high-speed camera and a high-speed static strain test analyzer with a synchronous control system (PC 1, PC 2, and an EF-500A-type high-energy pulse detonator). The instrument layout for the field experiments is shown in Figure 1, and the relevant experimental system is shown in Figure 2.

A high-speed camera (5KF10, Hefei Fuhuang Junda High-Tech Information Technology Co., Ltd., China) that can provide 1 million pixels, 3500 frames of shooting capability, and full-frame resolution (1280 × 860 pixels) for 4000 fps high-frame-rate images was used. The pixel size is 14 μm × 14 μm. The machine memory is 16 GB; 4 GB of images can be acquired per second, leading to an accuracy of 0.01 μs.

A high-speed static strain test analyzer (DH3820, Jiangsu Donghua Testing Technology Co., Ltd., China) combined with a foil resistance strain gauge sensor (BX120-20AA,

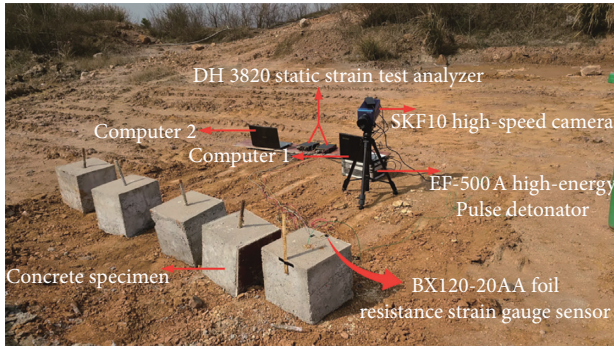


FIGURE 1: Experimental instrument layout in the field.

Beijing Yiyang Yingzhen Testing Technology Co., Ltd., (China) was used to collect data on the strain changes in the concrete model. The high-speed static strain test analyzer has a variable range of  $\pm 50000 \mu\epsilon$  and a maximum continuous sampling rate of 100 Hz/channel. The instrument is small, easy to use, and suitable for many environments, both indoors and out.

The foil resistance strain gauge sensor has a sensitivity coefficient of  $2.08 \pm 0.01 \Omega$ , a base size of  $26 \text{ mm} \times 6 \text{ mm}$ , and a sensitive column size of  $20 \text{ mm} \times 3 \text{ mm}$ , does not require any welding for use, and can detect a maximum microstrain of  $20000 \mu\epsilon$ . The self-contained insulated wire has a length of 20 cm and can be crimped to a custom conductor with a length of 0.2 cm to 2 m.

The synchronous control system was completed by a computer terminal and detonating device. The startup sequence and delay time of the detonation, shooting, and acquisition were defined, and control is possible to the microsecond. The high-speed camera and high-speed static strain test analyzer controlled by the computer terminal simultaneously photographed and measured the strain in the model specimens. Blasting tests were carried out in good lighting and stable exposure conditions.

### 3. Experimental Design

Boreholes in rock and rock-like materials will produce a large number of random cracks under a blast load, even with minimal amounts of explosive. These experiments aimed to study the impact of different filler media with varying decoupling coefficients on the blasting effect. The model material used was concrete, as this was expected to demonstrate the effects most successfully. Small concrete models constructed based on the blasting similarity criterion functioned as representative specimens. Concrete is convenient, economical, safe, and somewhat protective of the engineering site. The model specimen was a single-borehole charge containing 0.5 g diazodinitrophenol (DDNP) with a special small electric detonator measuring  $6 \text{ mm} \times 44 \text{ mm}$ . It was detonated by the high-voltage discharge of an EF-500A high-energy pulse initiator. Table 1 lists the relevant parameters of the concrete model specimen, and Table 2 lists the relevant parameters of the special electric detonator.

The model test piece was made of ordinary standard Portland cement (with a strength grade of 42.5 MPa), sand,

gravel, and water, which were mixed and stirred at a mass ratio of 1 : 1.556 : 3.158 : 0.52 and then maintained for 28 d at a temperature of  $20 \pm 2^\circ\text{C}$  and relative humidity of  $60\% \pm 5\%$ . The experimental model had a geometric similarity ratio of  $CL=0.1$ , and 30 concrete models with dimensions of  $300 \times 300 \times 300 \text{ mm}$  were produced based on the blasting similarity criterion, as shown in Figure 3. With the same method, three cylinders with a bottom diameter of 50 mm and a height of 100 mm were prepared to investigate the physical and mechanical properties of the model specimens, as shown in Figure 4.

A borehole was predrilled to a depth of 60 mm in the center of the specimen. Six specimens were prepared for each of the borehole diameters,  $d_B = 8, 10, 12, 14,$  and  $16 \text{ mm}$ . As only the decoupled charge structure was studied, the effects of five different decoupling coefficients on the blasting effect of air and EPS were explored. The EPS used in these experiments and its related material parameters are presented in Figure 5 and Table 3, respectively. As shown in Figure 6, the diameter was  $d_A = 6 \text{ mm}$ , and the borehole diameter varied as  $d_B = 8, 10, 12, 14,$  and  $16 \text{ mm}$ . The effects of air and polystyrene foam on the blasting effect were studied, and the corresponding decoupling coefficients were  $\alpha_A = \alpha_B = 1.33, 1.67, 2, 2.33,$  and  $2.67$ .

## 4. Experimental Procedures

4.1. *Geometric and Dynamic Elements of the Blast.* The experimental procedure to determine the blast geometry and speed was as follows:

- (1) Three concrete specimens with borehole diameters  $d_B = 8 \text{ mm}$  were used. One utilized the air-decoupled charge structure; the other two specimens used the EPS-decoupled charge structure. The specimens were charged and filled.
- (2) The high-speed camera was placed 3 m from the specimen and connected and powered on along with computer 1, and the collection parameters were defined (see Figure 2).
- (3) Once the personnel had been evacuated to the bunker, the detonation was started. The high-speed camera acquired images in a controlled fashion.
- (4) After the blast, the main geometric elements of the blasting funnel, including the blasting funnel radius, depth, and volume, were measured and recorded. The data from the high-speed camera were saved, the collection parameters were reset, and the next test was started.
- (5) Steps 1 through 4 were repeated for concrete specimens with diameters  $d_B = 10, 12, 14,$  and  $16 \text{ mm}$ . After the data collection, the data were sorted and analyzed.

4.2. *Strain Peak Tests and Block Degree Analysis.* The following experimental procedure was used to measure the strain:

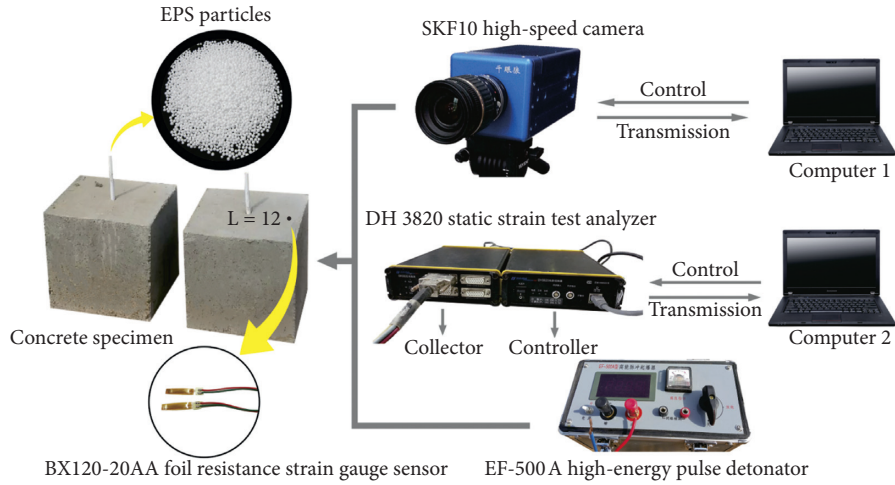


FIGURE 2: Schematic of the experimental system.

TABLE 1: Relevant material parameters of the concrete model.

Density ( $\text{g}/\text{cm}^3$ )	Dynamic elastic modulus (GPa)	Compressive strength (MPa)	Tensile strength (MPa)	Poisson's ratio	S-wave velocity (m/s)	P-wave velocity (m/s)
2.1	24.5	29.1	1.7	0.23	2095	3785

TABLE 2: Parameters for the DDNP special electric detonator.

Density ( $\text{g}/\text{cm}^3$ )	Detonation velocity (m/s)	Explosive heat (kJ/kg)	Dimensions (mm)
1.0	4500	4000	$6 \times 44$

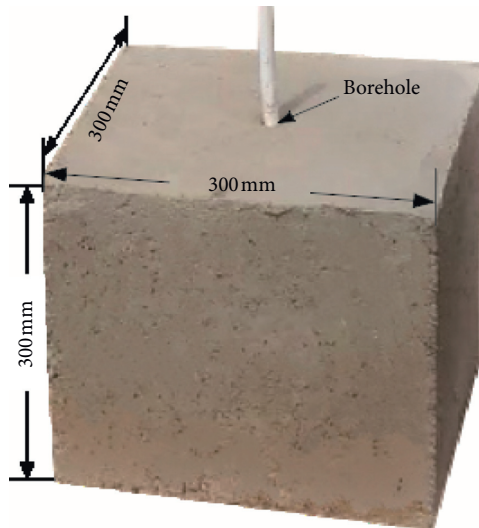


FIGURE 3: Concrete model specimen.

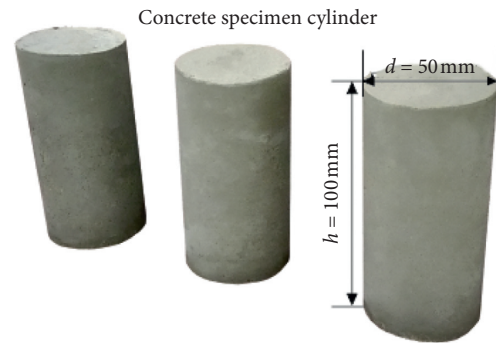


FIGURE 4: Concrete cylinder specimens.



FIGURE 5: EPS particles used in the experiments.

- (1) Three concrete specimens with borehole diameters  $d_B = 8$  mm were used. One utilized the air-decoupled charge structure; the other two specimens used the EPS-decoupled charge structure. The specimens were charged and filled.

TABLE 3: Relevant material parameters of EPS.

Density ( $\text{g/cm}^3$ )	Melting point temperature ( $^{\circ}\text{C}$ )	Resistivity ( $\Omega/\text{cm}$ )	Thermal expansion coefficient (K)
1.11–1.12	240	1020–1022	$8 \times 10^{-5}$

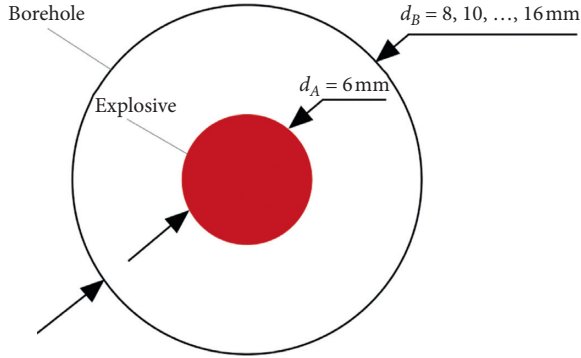


FIGURE 6: Diagram of the charge structure.

- (2) A foil resistance strain gauge sensor was tangentially attached to the top of the test piece at a distance of 12 cm from the center of the borehole. The high-speed static strain test analyzer and computer 2 were connected and powered on, and the parameters were defined (see Figure 2).
- (3) Once filled, the three model specimens were covered with a flexible protective cover to prevent the scattering and secondary crushing of fragments after the explosion. Once the personnel had been evacuated to the bunker, the detonation was carried out, and the static strain analyzer collected high-speed stress-strain data for the model specimen.
- (4) After the blast, the gravel in the flexible protective sleeve was collected, the block sizes of the gravel were classified using sieves with apertures of 10, 15, 20, 25, 30, and 40 mm, and the percentage of each fraction was calculated and recorded. The data were collected by the high-speed static strain tester, the collection parameters were reset, and the next test was started.
- (5) Steps 1 through 4 were repeated for concrete specimens with diameters  $d_B = 10, 12, 14, \text{ and } 16$  mm. After data collection was completed, the data were sorted and analyzed.

Two BX120-20AA strain gauges were bonded to the front surface of 15 concrete models in radial and tangential directions with superglue. The distance between the measurement point center and the center of the borehole was 12 cm, and the strain data for the concrete model specimens were collected by the static strain test analyzer. According to the experimental blasting scheme, 15 concrete models were tested for blasting and strain. Zero drift elimination and calibration of the instrument was required before each model test piece was tested.

## 5. Results and Analysis

**5.1. Geometric Elements of the Blasting Funnel.** The geometric elements of the blasting funnel, i.e., its radius, depth, and volume, were used to evaluate the blasting effect. Thirty groups of data for each index were obtained in the blasting experiments, with three groups for each index. To facilitate data processing and analysis, averages of the three data groups were taken to represent the index. The results for postblast indices of geometric elements were recorded, as listed in Table 4.

The relationships between the mean radius, depth, and volume of the blasting funnel and the decoupling coefficient were plotted using the data in Table 4, as shown in Figures 7(a)–7(c), respectively.

The relationship between the radius of the blasting funnel and the decoupling coefficient is shown in Figure 7(a). The radius of the blasting funnel initially increases and then decreases with an increase in the decoupling coefficient, which indicates that there is an optimal decoupling coefficient in the actual decoupled charge structure. In the decoupled charge structures with air and EPS as the filling media, the radius of the blasting funnel reached the maximum values with  $\alpha_A = 1.8\text{--}2.0$  and  $\alpha_P = 1.7\text{--}1.9$ , respectively. The decoupling coefficients were not in the same range, indicating that the influence of the two filling media on the blasting effect was inconsistent. The blasting funnel radius reached the optimal value for the air-decoupled charge structure at  $\alpha_A = 1.90$ , and the EPS-decoupled charge structure was optimal at  $\alpha_P = 1.76$ .

The variations in the depth of the blasting funnel (Figure 7(b)) and volume of the blasting funnel (Figure 7(c)) with the decoupling coefficient were similar to that of the blasting funnel radius (Figure 7(a)). Both initially increased and then decreased with an increase in the decoupling coefficient. This indicates that there were decoupling coefficients that corresponded to the optimal depth and volume of the blasting funnel in the actual decoupled charge structure. In the decoupled charge structure with air and EPS, when  $\alpha_A = 1.8\text{--}2.0$  and  $\alpha_A = 1.5\text{--}1.8$ , the depth and volume of the blasting funnel reached the maximum values, respectively. When  $\alpha_A = 1.87$  and  $1.90$  and  $\alpha_P = 1.54$  and  $1.75$ , the depth and volume of the blasting funnel reached the optimal values, respectively.

In the air-decoupled charge structure, a decoupling coefficient of 1.89 yielded the optimal values for each index of the blasting funnel. In the EPS-decoupled charge structure, the optimal value of the decoupling coefficient was 1.68. This shows that the EPS-decoupled charge structure can

TABLE 4: Experimental results for the geometric elements of the blasting funnel.

Decoupling coefficient	Filling medium	Radius of blasting funnel, $r$ (cm)			Average radius, $r$ (cm)			Depth of blasting funnel, $h$ (cm)			Average depth, $h$ (cm)			Volume of blasting funnel, $v$ (cm <sup>3</sup> )			Average volume, $V$ (cm <sup>3</sup> )
		Specimen 1	Specimen 2	Specimen 3	Specimen 1	Specimen 2	Specimen 3	Specimen 1	Specimen 2	Specimen 3	Specimen 1	Specimen 2	Specimen 3	Specimen 1	Specimen 2	Specimen 3	
1.33	Air	5.36	4.98	5.02	5.12	5.79	5.43	5.63	5.79	5.67	5.43	5.63	151.90	151.98	153.47	152.45	
	EPS	6.01	6.54	6.98	6.51	6.11	6.09	6.11	6.22	6.22	6.09	6.11	269.24	270.03	269.98	269.75	
1.67	Air	5.81	6.11	5.87	5.93	5.55	5.87	5.82	6.04	6.04	5.87	5.82	212.71	209.23	212.02	211.32	
	EPS	7.54	6.99	7.43	7.32	6.16	6.21	6.23	6.32	6.32	6.21	6.23	346.40	346.61	344.45	345.82	
2.00	Air	6.32	6.43	6.57	6.44	5.79	5.98	5.96	6.11	6.11	5.98	5.96	250.70	251.25	256.87	252.94	
	EPS	7.20	6.97	7.22	7.13	6.06	6.12	6.15	6.27	6.27	6.12	6.15	322.30	323.04	320.21	321.85	
2.33	Air	5.50	5.87	6.21	5.86	5.57	5.98	5.83	5.64	5.64	5.98	5.83	201.17	201.04	199.89	200.70	
	EPS	6.55	6.03	6.44	6.34	6.09	6.12	6.06	5.88	5.88	6.12	6.06	248.17	249.21	250.37	249.25	
2.67	Air	4.69	4.72	4.81	4.74	5.56	5.64	5.61	5.33	5.33	5.64	5.61	86.220	127.01	168.25	127.16	
	EPS	5.39	5.73	5.47	5.53	5.84	6.22	5.91	5.97	5.97	6.22	5.91	189.56	191.02	189.33	189.97	

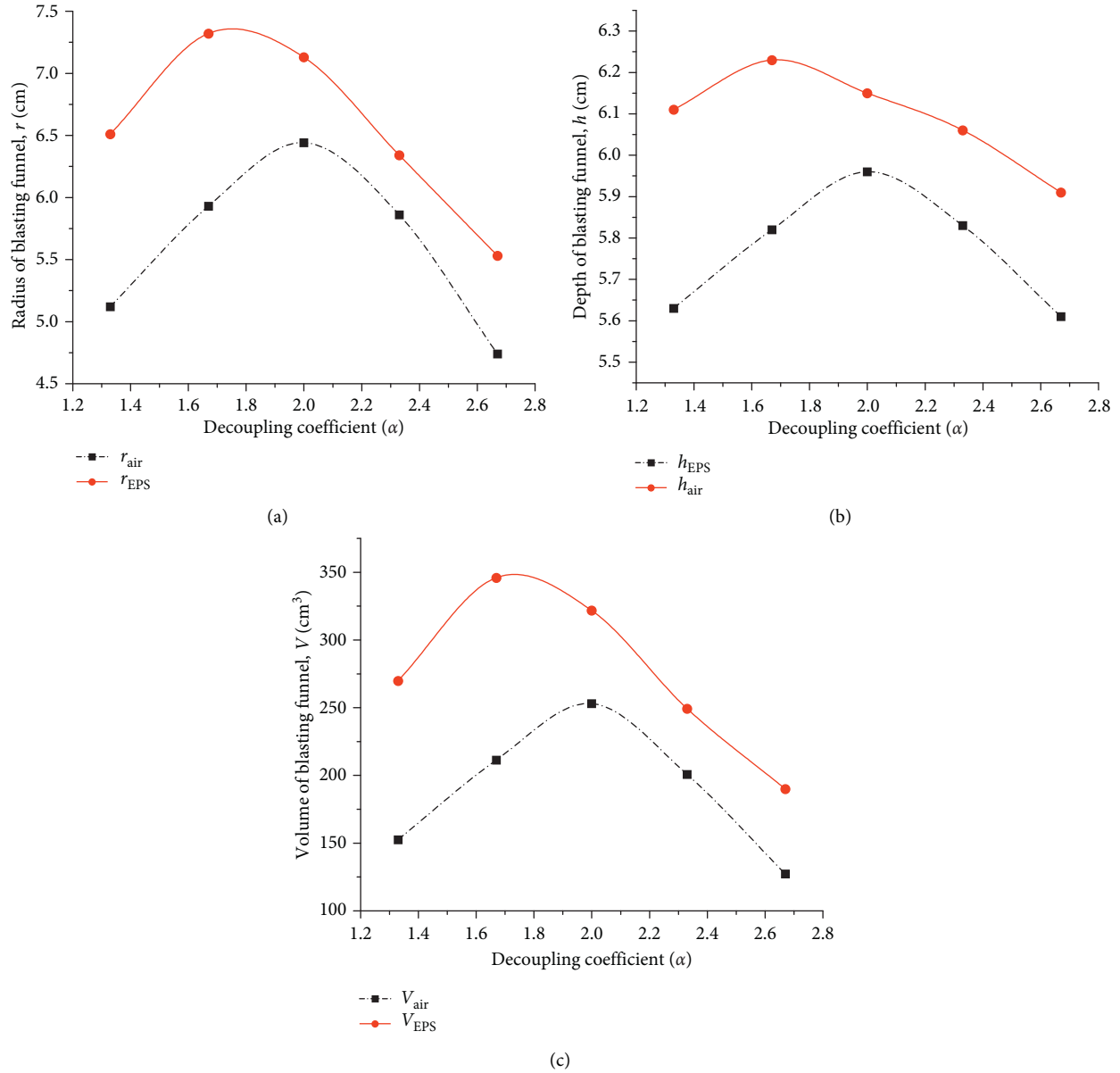


FIGURE 7: Relationships between geometric elements of the blasting funnel and the decoupling coefficient: (a) radius of the blasting funnel, (b) depth of the blasting funnel, and (c) volume of the blasting funnel.

achieve a better blasting effect with a smaller decoupling coefficient. It can be seen from Figures 7(a)–7(c) that the variations in the radius, depth, and volume of the blasting funnel with the decoupling coefficient all follow increasing first and then decreasing changing trend under the two different filling media. When the decoupled coefficient is the same, a large radius, depth, and volume after blasting with the EPS-decoupled charge and the blasting effect are better. In case of the EPS-decoupled charge structure, excessive pulverization of the near-field rock can be avoided by prolonging the action time of the blasting stress wave and the explosive gas, changing the specific gravity of the energy distribution, and using more blasting energy for crushing.

**5.2. Flyrock Launch Velocity.** The postblasting process can be divided into three stages: the stress wave tensile failure stage, explosive gas expansion crack stage, and the flyrock launch velocity stage. Only the flyrock launch velocity in the third stage was analyzed in these experiments by organizing and analyzing the data collected by the high-speed camera. The average value of the three flyrock launch velocities indicates the actual condition of the decoupled charge structure model specimens. The flyrock launch velocities of the model specimens after blasting are summarized in Table 5.

The variations in the flyrock launch velocity with the decoupling coefficient of the flyrock were plotted based on the results in Table 5. As shown in Figure 8, with the increase of the uncoupling coefficient, the flyrock launch velocity

TABLE 5: Flyrock launch velocities of the model specimens.

Decoupling coefficient	Filling medium	Flyrock launch velocity 1 $v$ ( $\text{ms}^{-1}$ )	Flyrock launch velocity 2 $v$ ( $\text{ms}^{-1}$ )	Flyrock launch velocity 3 $v$ ( $\text{ms}^{-1}$ )	Mean flyrock launch velocity 1 $v$ ( $\text{ms}^{-1}$ )
1.33	Air	6.54	6.65	6.43	6.54
	EPS	6.42	6.21	6.33	6.32
1.67	Air	6.35	6.50	6.56	6.47
	EPS	6.12	6.39	6.27	6.27
2.00	Air	6.53	6.45	6.31	6.43
	EPS	6.27	6.32	6.28	6.29
2.33	Air	6.63	6.33	6.57	6.51
	EPS	6.24	6.46	6.35	6.35
2.67	Air	6.50	6.63	6.79	6.63
	EPS	6.37	6.53	6.39	6.43

decreases first and then increases. The flyrock launch velocity initially decreases and then increases with an increase in the decoupling coefficient, and the variation trends for the two curves are the same. This indicates that there is a decoupling coefficient that optimizes the flyrock launch velocity in the actual decoupled charge structure.

For the same decoupling coefficient, the concrete model with the EPS-decoupled charge structure had a more moderate flyrock launch velocity after blasting was completed. A slower flyrock launch velocity could be obtained at a lower decoupling coefficient, as seen in Figure 8. The main reason for this phenomenon is that EPS is denser than air and has low compressibility. The energy of the explosive energy is transmitted to the distant rock medium; therefore, the explosive energy transmitted to the flyrock is lower, reducing the flyrock launch velocity. In the two decoupled charge structures, the minimum flyrock launch velocities occurred at  $\alpha_A = 1.75\text{--}1.95$  and  $\alpha_P = 1.51\text{--}1.61$ . The optimal decoupling coefficients were  $\alpha_A = 1.80$  and  $\alpha_P = 1.56$ .

**5.3. Peak Strain Values of the Specimens.** The radial, tangential, and mean strain data collected by the DH3820 system are summarized in Table 6.

From the five sets of radial decoupled charge blasting strain data results obtained in the tests, the relationships between the radial, tangential, and average strain and the decoupling coefficient are shown in Figure 9.

The radial and tangential peak strains initially increased and then decreased with an increase in the decoupling coefficient, as shown in Figure 9. This indicates that there is an optimal decoupling coefficient that can maximize the strain in the experimental model. With the same decoupling coefficient, the peak radial, tangential, and mean strains of the EPS-decoupled charge structure are higher than those of the air-decoupled charge structure. When the decoupling coefficient and filling medium are the same, the radial peak strain is greater than the tangential peak strain, and the model specimen with the EPS-decoupled charge structure exhibits a higher peak strain at a lower decoupling coefficient.

The corresponding peak strain is at its maximum when the radius and depth of the blasting funnel volume are at their maximum, as seen in Figures 7(a)–7(c) and Figure 9.

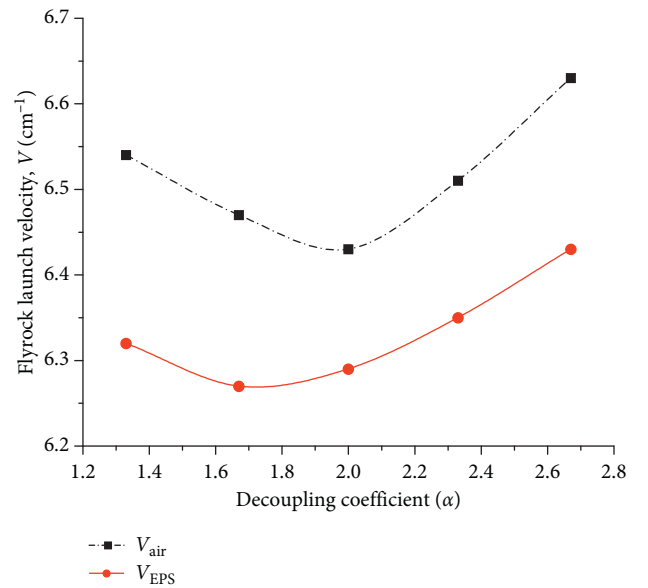


FIGURE 8: Relationship between the flyrock launch velocity and the decoupling coefficient.

For the air-decoupled charge structure, the maximum peak strain appears at  $\alpha_A = 1.80\text{--}1.95$ , and the optimal decoupling coefficient is 1.88. For the EPS-decoupled charge structure, the maximum peak strain appears at  $\alpha_P = 1.55\text{--}1.85$ , and the optimal decoupling coefficient is 1.80. For the same peak strain, the decoupling coefficient of the EPS-decoupled charge structure is smaller, indicating that the required drilled diameter is smaller. For the same decoupling coefficient, the peak strain of the EPS-decoupled charge structure is larger, which indicates that the blasting energy has a greater effect on the model specimens with the EPS-decoupled charge structure.

**5.4. Distribution of Gravel Lumpiness.** The degree of rock lumpiness after blasting is often used to evaluate the blasting effect. The gravel in the flexible protective sleeves was collected after the blasting and classified using sieves with apertures of 10, 15, 20, 25, 30, 35, and 40 mm. The percentage of gravel in each grade was calculated. The cumulative distributions of gravel lumpiness in each grade are shown in



TABLE 6: Peak strains of specimens with different filler media.

Decoupling coefficient	Filling medium	Directional strain		Mean strain ( $\mu\epsilon$ )
		Radial strain ( $\mu\epsilon$ )	Tangential strain ( $\mu\epsilon$ )	
1.33	Air	98.5	87.2	92.9
	EPS	122.4	115.3	118.9
1.67	Air	111.5	97.9	104.7
	EPS	162.4	147.1	154.8
2.00	Air	129.5	114.3	121.9
	EPS	150.8	134.0	142.4
2.33	Air	114.1	100.5	107.3
	EPS	136.6	117.4	122.0
2.67	Air	83.2	75.7	79.5
	EPS	104.4	90.2	97.3

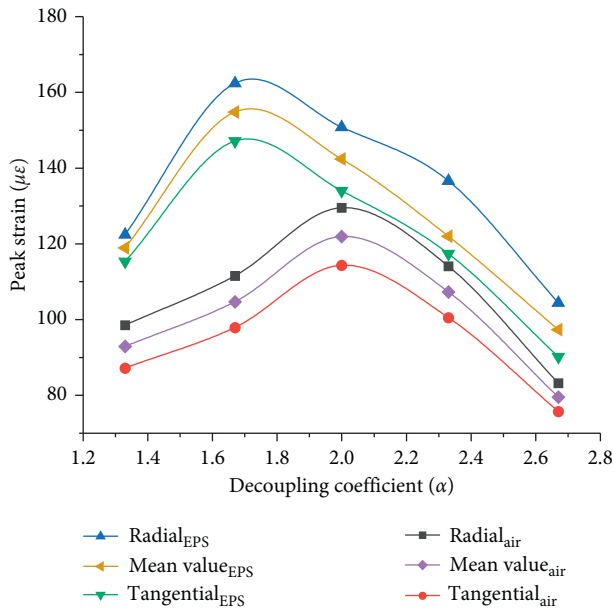


FIGURE 9: Peak strains of specimens with different filler media.

Table 7 for the model specimens with different charge structures.

The degree of fragmentation after blasting was analyzed with the G-G-S distribution function.  $K_{50}$  and  $K_{80}$  were used to evaluate the blasting effect. The G-G-S distribution function is expressed as follows:

$$\begin{aligned}
 y &= 100 \left( \frac{x}{x_0} \right)^n, \\
 K_{50} &= x_0 \left( \frac{1}{2} \right)^{(1/n)}, \\
 K_{80} &= x_0 \left( \frac{4}{5} \right)^{(1/n)},
 \end{aligned} \tag{1}$$

where  $y$  is the cumulative percentage of gravel under a certain sieve grade (%),  $x$  is the block size of the gravel (mm),  $x_0$  is the largest piece of gravel (mm),  $n$  is a distribution parameter, and the numerical values of distribution

parameters  $n$ ,  $K_{50}$ , and  $K_{80}$  are obtained via a regression method.

The statistical analysis of the gravel block size distribution is given in Table 8.

The relationships between the maximum gravel sizes,  $K_{50}$ ,  $K_{80}$ , and the decoupling coefficient of the specimens after blasting are plotted based on the data in Table 8, as shown in Figures 10(a) and 10(b).

The maximum gravel size initially decreased and then increased with an increase in the decoupling coefficient for the two decoupled charge structures, as shown in Figure 10(a). The EPS-decoupled charge structure had the maximum gravel size, which appeared at a smaller decoupling coefficient. Thus, the higher the decoupling coefficient of the air-decoupled charge structure, the larger the maximum gravel size of the model specimens.

The  $K_{50}$  and  $K_{80}$  index values of the EPS-decoupled charge structure are smaller than those of the air-decoupled charge structure, and the gravel lumpiness is more evenly distributed, as seen in Figure 10(b). The blasting effect of the EPS-decoupled charge structure is better than that of the air-decoupled charge structure. In the model specimens with the air-decoupled charge structure, the value of  $K_{50}$  varies from 40.22 to 83.81 mm. The size of the gravel is large, and the distribution is less concentrated. In the model specimens with the EPS-decoupled charge structure, the value of  $K_{50}$  varies from 31.20–44.39 mm, which is a large variation. The size of the gravel is smaller and the distribution is more even.

It can also be concluded that for the model specimens with different decoupled charge structures, the values of  $K_{80}$  vary from 59.42–116.91 mm and 45.40–75.39 mm, respectively, and the distribution trends are similar to the those for  $K_{50}$ , indicating that the energy of the explosive with the EPS-decoupled charge structure is more even. By avoiding the formation of crushing areas near the rock source, more explosive energy can be transferred to the rock medium in the distant source.

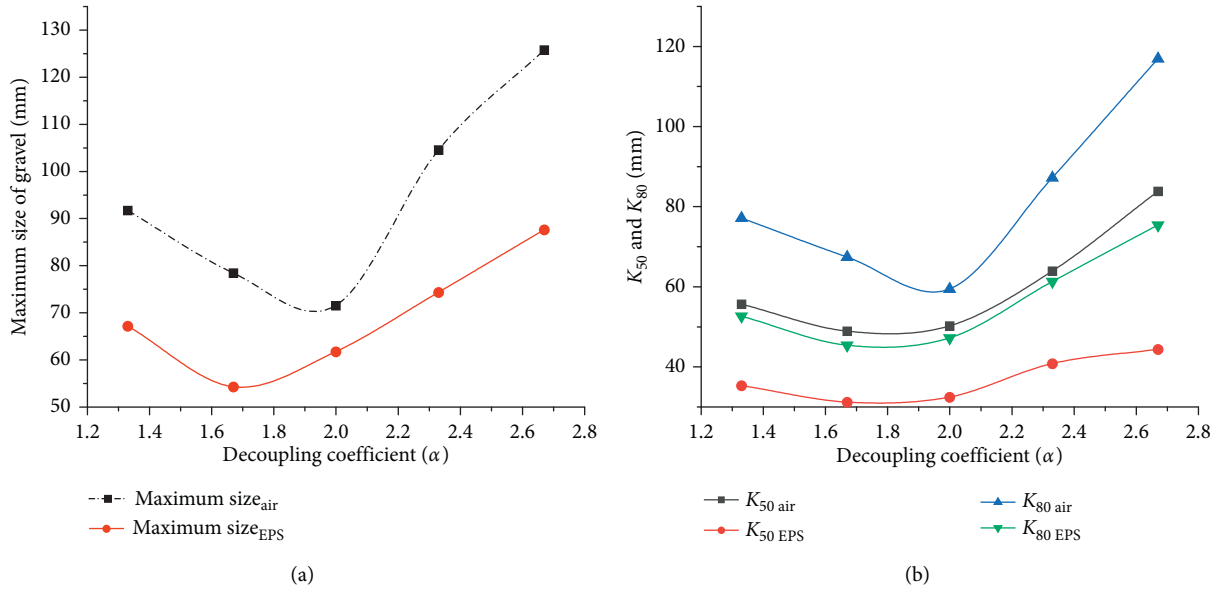
The maximum gravel size and  $K_{50}$  and  $K_{80}$  show a changing trend of decreasing first and then increasing with the increase of the decoupling coefficient, as shown in Figures 10(a) and 10(b). Thus, there is an optimal decoupling coefficient to achieve the desired blasting effect. In the model specimens with the air-decoupled charge structure, when  $\alpha_A = 1.80$ , the minimum value of  $K_{50}$  is 40.22 mm, and the

TABLE 7: Distribution of gravel lumpiness after blasting (%).

Decoupling coefficient	Filling medium	Block grade (mm)						
		<10	<15	20	<25	<30	<35	<40
1.33	Air	7.26	11.62	14.97	19.17	30.86	37.96	45.07
	EPS	9.37	18.49	23.15	29.37	38.69	48.40	58.10
1.67	Air	5.35	11.17	17.11	23.89	30.51	36.21	41.91
	EPS	11.31	25.09	32.86	42.57	53.64	60.19	66.74
2.00	Air	5.29	9.15	9.93	14.60	20.26	25.04	29.81
	EPS	11.50	22.76	29.95	35.09	44.51	48.64	52.76
2.33	Air	3.07	6.23	8.22	11.91	16.40	19.60	22.80
	EPS	8.98	15.68	18.69	23.73	34.80	40.63	46.45
2.67	Air	3.28	4.79	6.37	10.06	13.62	15.85	18.08
	EPS	11.89	20.63	24.03	31.60	44.90	50.05	55.19

TABLE 8: Statistical analysis of the block distribution of macadam.

Decoupling coefficient	Filling medium	Distribution parameter, $n$	Maximum gravel, $X_0$	$K_{50}$ (mm)	$K_{80}$ (mm)
1.33	Air	1.29	91.71	55.62	77.16
	EPS	1.08	67.19	35.32	52.62
1.67	Air	1.47	78.45	48.90	67.38
	EPS	1.25	54.26	31.20	45.40
2.00	Air	1.20	71.52	50.22	59.42
	EPS	1.08	61.73	32.45	47.18
2.33	Air	1.41	104.56	63.91	87.23
	EPS	1.16	74.33	40.80	61.28
2.67	Air	1.25	125.75	83.81	116.91
	EPS	1.02	87.60	44.39	75.39

FIGURE 10: Relationship between the decoupling coefficient and (a) the maximum gravel size and (b)  $K_{50}$  and  $K_{80}$ .

optimal decoupling coefficient is 1.73. In the model specimens with the EPS-decoupled charge structure, when  $\alpha_p=1.61$ , the minimum value of  $K_{50}$  is 31.20 mm, and the optimal decoupling coefficient is 1.66.

For  $K_{80}$ , the minimum values of the air-decoupled and EPS-decoupled charge structures are 59.42 and 45.40 mm,

respectively, and the optimal decoupling coefficients are 1.95 and 1.75, respectively. The comparison of the experimental results for the model specimens with two types of decoupled charge structures shows that the EPS-decoupled charge structure can effectively improve the distribution of gravel lumpiness and improve the utilization of explosive energy.

## 6. Discussion

The decoupling coefficients and the filling media have a significant impact on the blasting effect. Air and EPS have the same cushioning effect. However, different decoupling coefficients and filling media can result in different blasting effects and energy distributions. The experimental results are discussed and analyzed from the perspectives of the decoupling coefficients, filling media, and transmission and loss of blasting energy in this section.

**6.1. Decoupling Coefficients.** The decoupling coefficient strongly affected the blasting effect and energy transfer. With a small decoupling coefficient, the explosive energy acted almost directly on the borehole and formed a compressive crushing zone. The energy dispersed to distant areas was lessened, and the phenomenon of a high block rate was likely to occur. With a large decoupling coefficient:

- (i) The blast stress wave was transmitted for too long in the filling medium.
- (ii) Much of the explosive energy was consumed in the medium.
- (iii) The excess explosive energy acted on the borehole.
- (iv) The distant blasting area was unable to achieve the expected blasting effect.

In model experiments with two decoupled charge structures, when  $\alpha_A = 1.89$  and  $\alpha_P = 1.75$ , the radius, depth, and volume of the model blasting funnel reached the maximum values (see Figures 7(a)–7(c)).

When the decoupled coefficients were  $\alpha_A = 1.80$  and  $\alpha_P = 1.56$ , the flyrock launch velocities of the model specimens reached the minimum values (see Figure 8). With  $\alpha_A = 1.88$  and  $\alpha_P = 1.80$ , the peak values of the blasting stress in the model specimens were the highest (see Figure 9). When  $\alpha_A = 1.73$  and  $\alpha_P = 1.66$ , the maximum size of the gravel was at a minimum (see Figure 10(a)). Therefore, in the decoupled charge structure for the same rock type and explosive type, there was a specific decoupling coefficient that optimized the blasting effect.

Under the joint action of the blasting stress wave and blasting gas, the experimental results and decoupling coefficient show the changing trend of first increasing and then decreasing or first decreasing and then increasing, which indicates that the decoupling coefficient is an important factor influencing the blasting effect. In these experiments, the radius, depth, volume, and peak stress of the blasting funnel of the model specimens were optimal when the air-decoupled charge was equal to  $\alpha_A = 1.83$ . With EPS as the filling medium and a decoupling coefficient  $\alpha_P = 1.69$ , the initial flyrock launch velocity, maximum block size, and block rate of the model specimens were optimal. Thus, there was a specific decoupling coefficient that optimized the blasting effect.

Moreover, the decoupling coefficient was related to the type and nature of the filling medium. The blasting effect could be optimized with the selection of the filling medium and decoupling coefficient.

**6.2. Filling Medium.** In the blasting tests of model specimens with different filling media, the radius, depth, volume, and peak value of the obtained blasting funnel initially increased and then decreased with an increase in the decoupling coefficient (see Figures 7(a)–7(c)). The flyrock launch velocity and maximum flyrock block size initially decreased and then increased with an increase in the decoupling coefficient (see Figures 8 and 10(a)). It was found that the decoupled charge structure with EPS could increase the peak burst stress for a decoupling coefficient in the range of  $1.75 < \alpha < 2.05$  (see Figure 9), which is similar to the research reported by Yang et al. [21] ( $2.5 < \alpha < 2.35$ ), but the decoupling coefficient range is different. Yang et al. [21] chose a polycarbonate material (with a modulus of elasticity of 4.548 GPa, Poisson's ratio of 0.321, and density of 1449 g/cm<sup>3</sup>) and concrete (modulus of elasticity of 24.5 GPa, Poisson's ratio of 0.23, and density of 2100 g/cm<sup>3</sup>) as the model specimen materials; the different physical parameters of the two model specimens resulted in a difference in the range of the decoupling coefficient.

Owing to the high density of EPS, its compressibility was small and yielded better energy transfer. After the explosion, the gas in the polystyrene foam expanded more rapidly than that in the air, thereby reducing the flyrock launch velocity (see Figure 8). The EPS resulted in a more uniform and lower pressure on the borehole, which reduced the excessive pulverization around the borehole, avoided a high block rate, effectively improved the block distribution of the gravel, and made the utilization of the explosive energy more uniform and reasonable (see Table 8 and Figures 10(a) and 10(b)).

Comparing and analyzing the results of the two decoupled charge structure blasts, the blasting effect of the concrete model specimens with the EPS-decoupled charge structure was better. The optimal blasting effect could be obtained at a smaller decoupling coefficient.

The authors recommend reducing the diameter of the borehole to save engineering costs. The EPS-decoupled charge structure has many engineering advantages; there is no need for an auxiliary device to fix the position of the explosive in the borehole, which can reduce complicated construction links and achieve an ideal blasting effect in some blasting environments with special requirements.

The type of filling medium and decoupling coefficient can most effectively impact the blasting energy transfer characteristics.

**6.3. Blasting Energy Transfer and Loss.** EPS can be characterized as a lightweight material with strong shock absorption and high mechanical strength. Its self-shock period is long, which delays the blasting stress action time. Compared with a coupled charge structure, the decoupled charge structure prevents the blasting shock wave from directly acting on the borehole and transmits more blasting energy to a greater distance, thus achieving the best blasting effect.

The energy transfer losses stemmed from the lower compressibility of EPS; thus, the explosion in EPS was much lower than that in air. With EPS as the filling medium, the

energy consumed by deformation is less than that with air as the medium. The breaking energy not used on the rock is much lower than that with air. Because air has a high compression rate, much of the explosive energy is consumed by the compression of the air.

## 7. Conclusions

The effects of the filling medium and the decoupling coefficient on the blasting effect were investigated from the perspective of energy transfer and loss. In these experiments, concrete puckering decoupled blasting physical models were considered and a high-speed camera combined with a high-speed static strain testing analyzer was used. The authors then analyzed the geometric elements of the blasting funnels in the model specimens after blasting, the flyrock launch velocity, the peak strain of the specimens, and the distribution of the gravel lumpiness.

The filling medium had a significant effect on the blasting. The experimental results showed that the decoupled charge structure with EPS had a profound influence on the blasting effect in the concrete models.

At the same decoupling coefficient, for the EPS-decoupled charge structure,

- (i) The radius, depth, and volume of the blasting funnel were larger.
- (ii) The flyrock launch velocity was slower.
- (iii) The peak stress peak of the specimen was higher.
- (iv) The distribution of gravel was more even.

EPS is denser than air and much less compressible, which allowed for a more even pressure and a prolonged shock wave for an overall better energy transfer. There was less pulverization around the borehole, a lower block rate, improved block distribution, and better utilization of the explosive energy.

The decoupling coefficient significantly impacted the blasting effect, and there is a specific decoupling coefficient that could lead to an optimal blasting effect. The decoupling coefficient and the type and nature of the filling medium had an enormous influence on the blasting effect. The optimal decoupling coefficient for the air-decoupled charge structure was 1.83, whereas that of the EPS-decoupled charge structure was 1.69. The optimal blasting effect can be obtained by using EPS as the filling medium with a small decoupling coefficient.

The tests qualitatively compared the explosion effects of model specimens with different filling media and decoupling coefficients. The theoretical analysis and quantitative calculations were insufficient and obvious. Although five different decoupling coefficients were used in the experiments, the optimal decoupling coefficient for different decoupled charge structures was found only by curve fitting, which was limited by the cost of materials; thus, experimental calculation of the optimal decoupling coefficient was not performed. Specific experimental verification of the calculated optimal decoupling coefficient and a more in-depth study of the transfer of explosive energy with different charge

structure conditions are the main directions for future research.

## Data Availability

The data used to support the findings of this study are available from the corresponding author upon request.

## Conflicts of Interest

The authors declare that there are no conflicts of interest regarding the publication of this paper.

## Acknowledgments

This research was funded by the National Natural Science Foundation of China (nos. 50764001 and 52034004).

## References

- [1] P. K. Singh, M. P. Roy, and R. K. Paswan, "Controlled blasting for long term stability of pit-walls," *International Journal of Rock Mechanics and Mining Sciences*, vol. 70, no. 9, pp. 388–399, 2014.
- [2] T. A. Sethu, "Introduction of drill and blast utilizing pneumatic rock-drills in a Rwandan artisanal underground mine," *Journal of the Southern African Institute of Mining and Metallurgy*, vol. 117, no. 4, pp. 313–319, 2017.
- [3] A. Khademian and R. Bagherpour, "Environmentally sustainable mining through proper selection of explosives in blasting operation," *Environmental Earth Sciences*, vol. 76, no. 4, p. 166, 2017.
- [4] M. Cardu and J. Seccatore, "Quantifying the difficulty of tunnelling by drilling and blasting," *Tunnelling and Underground Space Technology*, vol. 60, pp. 178–182, 2016.
- [5] I. Ocak and N. Bilgin, "Comparative studies on the performance of a roadheader, impact hammer and drilling and blasting method in the excavation of metro station tunnels in Istanbul," *Tunnelling and Underground Space Technology*, vol. 25, no. 2, pp. 181–187, 2010.
- [6] P. Persson, N. Lundborg, and C. Johansson, "The basic mechanisms in rock blasting," *International Journal of Rock Mechanics and Mining Sciences*, vol. 2, 1970.
- [7] Z. Zhu, H. Xie, and B. Mohanty, "Numerical investigation of blasting-induced damage in cylindrical rocks," *International Journal of Rock Mechanics and Mining Sciences*, vol. 45, no. 2, pp. 111–121, 2008.
- [8] N. Li, L. J. Chen, and P. Zhang, "Dynamic analysis for fracturing progress by detonation gas," *Chinese Journal of Geotechnical Engineering*, vol. 28, no. 4, pp. 460–463, 2006, in Chinese.
- [9] X. Lou, Z. Wang, B. Chen, and J. Yu, "Theoretical calculation and experimental analysis on initial shock pressure of borehole wall under axial decoupled charge," *Shock and Vibration*, vol. 2018, Article ID 7036726, 2018.
- [10] Y. Shu, P. Shao, C. Dong, Z. Cao, and X. Yi, "Influence of rock strength on the propagation of slotted cartridge blasting-induced directional cracks," *Advances in Civil Engineering*, vol. 2019, Article ID 5752189, 2019.
- [11] H. Draganić and D. Varevac, "Analysis of blast wave parameters depending on air mesh size," *Shock and Vibration*, vol. 2018, Article ID 3157457, 2018.

- [12] D.-Z. Kong, Z.-B. Cheng, and S.-S. Zheng, "Study on the failure mechanism and stability control measures in a large-cutting-height coal mining face with a deep-buried seam," *Bulletin of Engineering Geology and the Environment*, vol. 78, no. 8, pp. 6143–6157, 2019.
- [13] J. Ge and Y. Xu, "A method for making transparent hard rock-like material and its application," *Advances in Materials Science and Engineering*, vol. 2019, Article ID 1274171, 2019.
- [14] Z. Song, J. Mao, X. Tian, Y. Zhang, and J. Wang, "Optimization analysis of controlled blasting for passing through houses at close range in super-large section tunnels," *Shock and Vibration*, vol. 2019, pp. 1–16, 2019.
- [15] W. M. Liang, H. Y. Liu, and F. J. Zhou, "Influence of air-decoupled charge on rock blasting," *Advances in Materials Science and Engineering*, vol. 32, no. 12, pp. 1215–1218, 2012, in Chinese .
- [16] W. Gu, Z. Wang, J. Chen, J. Liu, and M. Lu, "Experimental and theoretical study on influence of different charging structures on blasting vibration energy," *Shock and Vibration*, vol. 2015, p. 11, Article ID 248739, 2015.
- [17] Y. Lei, J. Liu, S. Zhang, W. Zhang, and H. Wang, "Contrast test of different permeability improvement technologies for gas-rich low-permeability coal seams," *Journal of Natural Gas Science and Engineering*, vol. 33, pp. 1282–1290, 2016.
- [18] Y. Wang, "Study of the dynamic fracture effect using slotted cartridge decoupling charge blasting," *International Journal of Rock Mechanics and Mining Sciences*, vol. 96, pp. 34–46, 2017.
- [19] P. F. Jiang, D. G. Tang, and L. Yuan, "Numerical analysis of influence of decoupled explosive-charge structure on stress field in hard rocks," *Rock Soil Mechanism*, vol. 30, no. 1, pp. 275–279, 2009, in Chinese.
- [20] W. Wang and X. C. Li, "Experimental study of propagation law of explosive stress wave under condition of decouple charge," *Rock Soil Mechanism*, vol. 31, no. 6, pp. 1723–1728, 2010, in Chinese.
- [21] R. Yang, C. Ding, L. Yang, Z. Lei, and C. Zheng, "Study of decoupled charge blasting based on high-speed digital image correlation method," *Tunnelling and Underground Space Technology*, vol. 83, pp. 51–59, 2019.
- [22] Z. X. Zhang, *Rock Fracture and Blasting: Theory and Applications*, Elsevier, Berlin, Germany, 2016.
- [23] W. Wang, X. C. Li, L. Shi, and Z. M. Fang, "Discussion on decoupled charge loosening blasting in deep rock mass," *Rock Soil Mech*, vol. 29, no. 10, pp. 2837–2842, 2008, in Chinese.
- [24] Z.-L. Wang, Y.-C. Li, and R. F. Shen, "Numerical simulation of tensile damage and blast crater in brittle rock due to underground explosion," *International Journal of Rock Mechanics and Mining Sciences*, vol. 44, no. 5, pp. 730–738, 2007.
- [25] L. P. Gorbachev and T. A. Semenova, "Estimate of geomagnetic disturbances in the presence of decoupled," *Atomic Energy*, vol. 89, no. 5, pp. 931–936, 2000.
- [26] M. S. Zhong, Y. Long, X. H. Li, L. Z. Shao, and Q. M. Xie, "Time function for borehole explosive loading and specific energy based on different coupled mediums," *Journal of Rock Mechanics and Geotechnical Engineering*, vol. 30, no. 7, pp. 116–119, 2011, in Chinese.
- [27] N. Bozorgzadeh and J. P. Harrison, "Reliability-based design in rock engineering: application of Bayesian regression methods to rock strength data," *Journal of Rock Mechanics and Geotechnical Engineering*, vol. 11, no. 3, pp. 612–627, 2019.
- [28] N. Yazdani, E. Beneberu, and M. Riad, "Nondestructive evaluation of FRP-concrete interface bond due to surface defects," *Advances in Civil Engineerin g*, vol. 2019, p. 10, 2019.
- [29] Z. L. Wang and B. Zhu, "Numerical analysis on energy-absorption of expanded polystyrene foam in radical decoupled Blast," *Natural Science*, vol. 10, no. 7, pp. 1020–1026, 2012, in Chinese.
- [30] W. J. Yang and Z. L. Wang, "Numerical study on blasting response of EPS foam decoupled charge in rock mass," *Journal of China Coal Society*, vol. 36, no. S2, pp. 425–430, 2011, in Chinese.